Study on the Therapeutic Mechanism of LXGYD on Intestinal Stem Cells and Tight Junction Proteins in GI-ARS Rats

Ziqiao Yan
Medical School of Chinese PLA: Chinese PLA General Hospital https://orcid.org/0000-0003-1837-7255
Bofeng Yin
Beijing Institute of Radiation Medicine
Yuguo Wang
Sixth Medical Center of PLA General Hospital
Jian Feng
PLA 96604 Hoapital, Lanzhou, CHINA
Qianyu Yang
Hebei University of Chinese Medicine
Xiao Li
Medical School of Chinese PLA: Chinese PLA General Hospital
Heng Zhu
Beijing Institute of Radiation Medicine https://orcid.org/0000-0002-8408-3821
Yongqi Dou (dyqi_301@yeah.net)
PLAGH: Chinese PLA General Hospital https://orcid.org/0000-0003-3611-8441

Research Article

Keywords: Chinese herbal medicine, GI-ARS, intestinal stem cell, Liangxue-Guyuan-decoction

Posted Date: December 1st, 2021

DOI: https://doi.org/10.21203/rs.3.rs-1112710/v1

Abstract

Background: Gastrointestinal acute radiation injury syndrome (GI-ARS) is potentially lethal and may occur after exposure to high radiation doses. Various chemical and biological agents have been developed to treat GI-ARS. However, their clinical utility is limited as they induce serious adverse reactions at their effective doses. Chinese herbal medicines have attracted attention because of their protective efficacy and low toxicity in radiation exposure treatment. However, their cellular and molecular mechanisms remain unknown. Here, we investigated the effects of the Chinese herbal Liangxue-Guyuan-Yishen decoction (LXGYD) on the intestinal stem cells and signal pathways of a GI-ARS rat model. Currently, there are limited treatment methods available globally; LXGYD might be a potential therapeutic option for patients with GI-ARS.

Methods: The rat GI-ARS model was prepared by whole-body irradiation with 10-Gy of ^{60}Co-γ rays. Various LXGYD concentrations were intragastrically administered to the irradiated rats. Health status and survival of the rats were evaluated and the protective efficacy of LXGYD on the intestines was assayed by pathological analysis. The active principles in LXGYD were detected by liquid chromatography-mass spectrometry (LC-MS) and their potential targets and pathways were screened by network pharmacological analysis. Intestinal stem cell proliferation, intestinal epithelial tight junction (TJ) protein expression, and regulatory pathways were explored by immunohistochemistry (IHC), western blotting (WB), and real-time quantitative polymerase chain reaction (RT-qPCR), respectively.

Results: LXGYD administration significantly improved health status and survival in GI-ARS rats. The pathological analysis showed that LXGYD ameliorated radiation-induced intestinal injury. The LXGYD infusion significantly promoted LGR5^{+} stem cell regeneration in the ileal crypts, upregulated TJ proteins, and accelerated crypt reconstruction in the irradiated rats in a dose-dependent manner. LC-MS revealed ≥ 13 LXGYD constituents that might contribute to its protective effects. Involvement of the WNT and MEK/ERK pathways in intestinal repair and recovery were screened by network pharmacology analysis and validated by western blotting.

Conclusions: The present study disclosed a heretofore unrecognized role of the Chinese herbal LXGYD in rescuing the intestinal stem cells of a GI-ARS rat model. It also showed that the WNT and MEK/ERK pathways may be involved in LXGYD-mediated intestinal regeneration in GI-ARS.

Introduction

Short-term exposure to high-dose irradiation can cause gastrointestinal acute radiation injury syndrome (GI-ARS) and it is also one of the most common complications in patients with abdominal radiation therapy[1]. This disorder damages the intestinal structure, induces severe symptoms, and may cause death. However, very few efficacious treatment strategies are currently available for GI-ARS. As they appear, symptoms are managed by fluid and electrolyte balance maintenance, blood transfusions, and antibiotics. Several chemical and biological compounds have been evaluated for GI-ARS therapy. Qiu et

al.[2] reported that insulin-like growth factor 1 (IGF-1) and basic fibroblast growth factor (bFGF) protected mouse intestines against radiation-induced apoptosis by suppressing the BH3-only protein p53 upregulated modulator of apoptosis (PUMA) via the PI3K/AKT/p53 axis. Liang et al.[3] demonstrated that cyclin-dependent kinase 4/6 inhibition with PD0332991 protected mouse intestines against lethal radiation-induced damage. Bhanja et al.[4] showed that the antineoplastic agent BCN057 promoted intestinal epithelial repair in irradiated mice. However, no drug has yet been approved by the US FDA for GI-ARS therapy mainly because the candidate therapeutic agents that have been assessed were highly toxic at their effective concentrations[5].Therefore, the purpose of this study was to develop a potential treatment strategy for GI-ARS.

Chinese herbal prescriptions have attracted attention for the treatment of radiation-induced injury as they are efficacious and have low toxicity. Wang et al.[6] demonstrated that the Chinese herbal prescription known as YiqiJiedu decoction significantly ameliorated radiation-induced testicular injury in mice by upregulating Toll-like receptor 5 (TLR5) expression in the testis and mitigating spermatogenic cell apoptosis. Other studies showed that various natural exact plant-derived products contribute to the protective effect against radiation damage. Cordycepin is an adenosine derivative that inhibits radiation-induced ulceration by upregulating nuclear factor erythroid 2-related factor 2 (NRF2) and preventing cell senescence[7]. Our recent research showed that natural exact ferulic acid promoted post-irradiation bone defect repair by maintaining skeletal stem cell stemness[8]. Other studies indicated that mitogen-activated protein kinase (MAPK) pathway activation was implicated in the protective mechanism of ferulic acid[9], [10]. Therefore, the discovery of novel herbal medicines and elucidation of their underlying radioprotective modes of action are medically relevant pursuits.

According to traditional Chinese medicine theory, acute radiation injury is a heat toxin and consumes ShenJing (ShenJing can be interpreted as kidney essence, which is the primitive material that constitutes the material base of the human body in the TCM theory) of the “Shen” system. According to TCM, the concept of the kidney ("Shen") differs from that of Western medicine, since "Shen" describes a set of interconnected parts and not just the anatomical organ.”. In TCM, the Chinese herbal Liangxue-Guyuan-Yishen decoction (LXGYD) is prescribed and administered for radioprotection. Our preliminary study[11] showed that LXGYD alleviated radiation-induced intestinal injury in rats partially by regulating the TLR4/myeloid differentiation primary response 88 (MyD88)/nuclear factor-kappa B (NF-κB) pathway. However, their cellular and molecular mechanisms and the active principles contributing to the radioprotective effects of LXGYD are unknown. In the current study, LXGYD compounds were screened by liquid chromatography-mass spectrometry (LC-MS) and the potential targets and pathways of the protective effects were identified by network pharmacological analysis. We also evaluated the impact of LXGYD and its constituents on ISC proliferation and TJ protein expression as these processes were previously reported to be involved in ileal crypt reconstruction.

Methods

Decoction preparation

All TCM materials were purchased from Beijing Tong Ren Tang Group (Beijing, China) and decocted twice. For the first decoction, the medicinal material was submerged in cold water and soaked for 30–60 min. Then, the water was decanted, and the medicinal material was placed in a casserole or ceramic pot. The vessel was then placed on fire, and the medicinal material was brought to boil, following which, the heat was turned down, and the medicinal material continued to decoct for 30 min. The first decocted liquid was then decanted. For the second decoction, the medicinal materials were submerged in hot water. The heat was turned up, and the mixture was boiled. The heat was then lowered, and the mixture was decocted for 20 min. The second decocted liquid was then decanted. The mixture was frequently stirred during both decoctions. Both decoctions were mixed, and the decocted liquid was placed in a rotary evaporator (Hei-VAP Core, Heidolph Instruments, Schwabach, Germany) and concentrated according to the corresponding proportions. The M D and H D liquids were sealed, stored at 4 °C, and heated to 30–40 °C before intragastric administration to the experimental animals.

Untargeted liquid chromatography-mass spectrometry (LC-MS) analysis

The foregoing compound was analyzed by LC-MS. All chemicals and solvents were analytical or HPLC grade. Methanol, acetonitrile, formic acid, and water were purchased from Merck KGaA (Darmstadt, Germany). The 2-chlorophenylalanine was acquired from GL Biochem (Shanghai, China). The devices used were: Vortex oscillator (TYXH-1; ZOLLO, Shanghai, China), High Speed Benchtop Refrigerated Centrifuge (TGL-16MS; LUXIANGYI, Shanghai, China), High Performance Liquid Chromatography system (Acquity UPLC/HPLC; Waters, USA), HPLC column (Acquity UPLC HSS T3; Waters), Mass Spectrometer (Q Exactive™ Plus Hybrid Quadrupole-Orbitrap™; ThermoFisher, US), and centrifuge (Sigma 1-16K, Sigma,-Aldrich, Darmstadt, Germany).

The sample was thawed slowly on ice, and 0.5 mL of it was freeze-dried. Then 800 µL of 80% (v/v) methanol was added to each sample. The samples were then mixed by vortexing, ultrasonicated at 4 °C for 30 min, cooled to -40 °C for 1 h, vortexed for 30 s, maintained at 4 °C for 30 min, and centrifuged at 10,800 × g for 15 min at 4 °C. Then 5 µL internal standard (0.14 mg/mL dichlorophenylalanine) was added to 200 µL supernatant, and the mixture was transferred to a liquid chromatography (LC) vial. The vials were stored at -80 °C until the LC-MS analysis.

The chromatographic conditions were as follows: column temperature, 40 °C; mobile phase A, 0.05% (v/v) formic acid; mobile phase B, acetonitrile solution; flow rate, 0.3 mL/min; sample volume, 3 µL; and automatic sampler temperature, 4 °C. The MS conditions in positive mode were as follows: heater temperature, 300 °C; sheath gas flow rate, 45 arb; auxiliary gas flow rate, 15 arb; tail gas flow rate, 1 arb; electrospray voltage, 3.0 kV; and capillary temperature, 350 °C; The MS conditions in negative mode were as follows: heater temperature, 300 °C; sheath gas flow rate, 45 arb; auxiliary gas flow rate, 15 arb; tail gas flow rate, 1 arb; electrospray voltage, 3.2 kV; and capillary temperature, 350 °C. Scanning mode: the first-level full scan range was m/z 70–1,050. For the data-dependent second-level MS (DD-MS2; TOPN =

10), the resolutions were 70,000 (primary MS) & 17,500 (secondary MS). Collision mode: high energy collision dissociation (HCD) was used.

Compound Discoverer v. 2.0 (Thermo Fisher Scientific, Waltham, MA, USA) was used to extract and preprocess the LC/MS detection data. The data were retrieved with the Orbitrap Traditional Chinese Medicine Library (OTCML; Thermo Fisher Scientific), normalized and post-edited in Microsoft Excel 2010 (Microsoft Corp., Redmond, WA, USA), and organized into a 2D data matrix comprising the molecular weight (MW), mass/charge ratio (m/z), retention time (RT), peak strength, and database-matching results. A TIC diagram of the LC/MS in the positive and negative ion modes is shown in Supplementary Fig. S1.

Network pharmacological analysis

The components with the highest content in the foregoing samples were selected using an *in silico* ADME model in the Traditional Chinese Medicine Systems Pharmacology (TCMSP) database. The latter compared and queried each component. Unique molecular ID and relative target information were obtained. Duplicate components and those with no corresponding ID were removed. Ingredients with unique molecular ID in the top 50 positive and negative ion modes were obtained. The ADME system used here predicted oral bioavailability (OB) and drug-likeness (DL). Compounds were retained only if their OB $\geq$ 30% and their DL $\geq$ 0.18 based on the criteria set by the TCMSP v. 2.3 database (https://tcmsp-e.com). A TCMSP target prediction model was used to forecast the putative target proteins of each active component. The names of the foregoing target proteins were retrieved from the Uniprot database (https://www.uniprot.org). The qualifier used was “confirmed” on a species that was “human.” The generic names of the genes corresponding to the target proteins were identified. The data were imported into Cytoscape v. 3.8.2 (https://cytoscape.org/download.html) to construct a drug-component-target-pathway network. The output was presented as an intuitive network graph.

Radiation-induced intestinal injury was searched in the GeneCards (https://www.genecards.org) and OMIM (https://www.omim.org) databases to obtain the genes associated with acute intestinal radiation injury. The online Wayne figure tools (https://bioinfogp.cnb.csic.es/tools/venny/) was used to screen for intersections among the target genes of the active ingredients in the compound and the genes related to acute intestinal radiation damage. In this manner, potential targets for the treatment of acute intestinal radiation damage might be detected. The intersecting genes were entered into the String (https://string-db.org) database to obtain protein-protein interactions (PPI) plots. The network view summarized the predicted association networks with other proteins. The nodes represented the proteins while the edges represented the predicted functional associations. The node size reflected the interaction levels in the network. The data were downloaded from the String database into Cytoscape 3.8.2 to plot a target-path network graph. The Metascape (ttps://metascape.org/gp/index.html#/main/step1) database was used for the gene ontology (GO) and Kyoto Encyclopedia of Genes and Genomes (KEGG) analyses. Cytoscape 3.8.2 was used to plot the drawings.

Animals and radiation source

Eighty-five specific pathogen-free male Sprague-Dawley (SD) rats with body weight in the range of 280–300 g were purchased from SPF (Beijing) Biotechnology Co. Ltd., Beijing, China. All animal experiments complied with relevant experimental animal welfare principles, which were approved by the Ethics Committee of the Academy of Military Medical Science, Beijing, China (No. IACUC-DWZX-2020-783). All experimental animals were maintained in a room at the Experimental Animal Center of the Academy of Military Medical Sciences. The relative humidity was 55 ± 2%, the temperature was 25 ± 2 °C, and the photoperiod was 12 h light/12 h dark. The γ-radiation source was ^{60}Co, and it was procured from the Institute of Radiation and Radiation Medicine of the Academy of Military Medical Sciences. The rats with very poor survival status and abdominal aorta blood were euthanized by a peritoneal overdose of pentobarbital sodium (100 mg/kg, IV). Unless otherwise specified, each experiment was performed in triplicate.

Experimental grouping

Eighty-five male SD rats each weighing 280–300 g were randomly assigned to one of the five following groups: control (Control), model (Radiation), positive drug (Gln), medium-concentration decoction (M D), and high-concentration decoction (H D). The rats used in the survival analysis were randomly assigned to one of the five foregoing groups. All groups except the Control had 12 rats. The Control had only five rats. After adaptive feeding for 3 d, the rats were fasted for 8 h before irradiation. Except for the Control, all groups were subjected to a single whole-body irradiation with 10-Gy of ^{60}Co γ-rays. The acute intestinal radiation injury assessments focused on the duodenum and terminal ileum alone as these parts of the small intestine are less physiologically active than the rest of the small intestine and are, therefore, more likely to receive the full radiation dose. This study conformed to the 3R principle, and we tried to optimize the experimental scheme.

In vivo drug administration

The LXGY decoction consisted of ginseng radix, astragalus membranaceus, water cow's horn, tree peony bark, dan-shen root, tractylodes atractylodes, pueraria root, rehmanniae glutinosa, rhizoma coptis, and other ingredients. The Chinese herbal decoction pieces were decocted twice. The M D and H D treatments were concentrated to 2.73 g/mL and 5.46 g/mL crude Chinese herbal medicine, respectively, at double and quadruple the equivalent doses administered to adult humans, respectively. They were stored at 4 °C until later use. The positive drug was glutamine in capsule form (Jiangsu Shenhua Pharmaceutical Co., Jiangsu, China). The contents of the glutamine capsule were mixed with 0.9% (w/v) physiological saline to make a 3 g/kg suspension for intragastric administration.

Western blotting

Radioimmunoprecipitation assay (RIPA) buffer and cocktail protease and phosphorylase inhibitors (Servicebio, Hubei, China) were added to rat jejuna, and the tissues were homogenized at 4 °C using a low temperature crushing homogenizer (JXFSTPRP-I-02, JINGXIN, Shanghai, China) and centrifuged at 4 °C ,12,000 × g for 5 min (Centrifuge 5425, Eppendorf, Germany). The supernatants were conserved, and

protein loading buffer (Servicebio, Wuhan, China) was added to them. The proteins were separated by 10% sodium dodecyl sulfate-polyacrylamide gel electrophoresis (SDS-PAGE) and transferred to a nitrocellulose membrane. The membrane was incubated with anti-β-Catenin, anti-C-MYC, and anti-phospho-MEK (anti-p-MEK), anti-MEK, anti-phospho-ERK (anti-p-ERK), anti-ERK, anti-GAPDH (Cell Signaling Technology, Danvers, MA, USA), and anti-WNT3A antibodies (Zen-Bioscience; www.zen-bio.cn) and incubated at 4 °C overnight. The membrane was then rinsed in Tris/Tween-20 buffer (TBST; Servicebio, Wuhan, China) and incubated with horseradish peroxidase (HRP)-bound secondary antibodies. The bands of Western blotting are displayed and analyzed by imaging system (ChemiDoc Imaging System 12003153-S, BIO-RAD, US).

RT-qPCR

RT-qPCR was performed to elucidate the Wnt pathway of the intestinal stem cells. The intestinal tissue was homogenized with RNA extraction compound (G3013; Wuhan ServiceBio Technology Co. Ltd., Wuhan, China). Reverse transcription was performed with a ServiceBio® RT First-Strand cDNA Synthesis Kit (G3330; Wuhan ServiceBio Technology Co.) according to the manufacturer's instructions. The cDNA was amplified by RT-qPCR. The primers were synthesized by Invitrogen (Carlsbad, CA, USA) and are listed in Supplementary Table S3. The mRNA levels were normalized to glyceraldehyde-3-phosphate dehydrogenase.

Hematoxylin-eosin (HE) staining and immunohistochemistry (IHC)

Five rats were randomly selected at days 3, 5, and 10 after irradiation. After the blood was collected from the abdominal aorta, the rats were euthanized as described previously. Small intestines were excised, and 3 cm of the upper segment of each jejunum was immersed in 4% (v/v) paraformaldehyde (PFA) for 72 h. The jejuna were sectioned into 5-μm slices, embedded in paraffin, and subjected to HE staining.

The jejunum paraffin sections were rehydrated in 100%, 95% (v/v), and 80% (v/v) ethanol for 10 min per treatment and rinsed with phosphate-buffered saline (PBS). The samples were incubated with 1% (v/v) bovine serum albumin (BSA) at room temperature (25–27 °C) for 30 min, subjected to primary antibody, incubated at 4 °C overnight, and washed thrice in PBS. The corresponding secondary antibody was applied to the samples, and they were incubated in a thermostatic chamber at 37 °C for 30 min. The samples were then rinsed thrice in PBS, rinsed with distilled water, and re-stained with hematoxylin. The samples were then dehydrated and sealed. Thirty intact crypts or villi were counted per section. The numbers of positive cells per crypt or villus were reported as means ± standard deviation (SD). At least five rats were used per group. The antibodies used were anti-Lgr5 (Novusbio, US), anti-CyclinD1 (Servicebio, Wuhan, China), anti-claudin-1 (Servicebio, Wuhan, China), and anti-occludin (Servicebio, Wuhan, China).

HE staining and IHC analyses

HE and IHC staining of the small intestine were observed under a microscope (Leika, Germany). For each group, suitable fields of vision for each tissue section were photographed using imaging software (Leika, Germany). The entire field of view was filled with tissue image to ensure uniform background lighting for all pictures. Villus length (μm) and crypt depth (μm) were measured with ImagePro Plus v. 6.0 (Media Cybernetics Inc, Rockville, MD, USA) for ≥ 5 sections per time point per group. The lower right corner scale was the standard. The IHC results were semi-quantitatively analyzed using ImageJ (Java 1.8.0_172, National Institutes of Health, Bethesda, MD, USA). The foregoing measurements were independently made by three observers blinded to the treatments.

Enzyme-linked immunosorbent assay (ELISA)

Except for the Control, five rats were randomly selected per group and per time point and ≥ 3 mL blood was drawn from each abdominal aorta. The blood was stored at room temperature and centrifuged at 4,000 × g for 15 min at 4 °C. The supernatants were collected and stored at -80 °C until the ELISA was performed with a Rat *D*-Lactate ELISA Kit (Shanghai Xin Fan Biotechnology Co. Ltd., Shanghai, China). The *D*-lactate standard was diluted and added to the test kit plate according to the manufacturer's directions. The diluted sample was added to the plate hole, and the corresponding solution was added to the sample and mixed with it. The mixture was incubated for 30 min, and the assay was conducted. A standard curve was plotted using the absorbances of a *D*-lactate standard dilution series, and the *D*-lactate concentration of each sample was interpolated from the graph based on the sample absorbance.

Statistical analysis

SPSS v. 19.0 (IBM Corp., Armonk, NY, USA) was used to analyze the data which were expressed as means ± SD. The repeated-measurement statistical method was used to analyze the data at various time points per group. $P < 0.05$ indicated statistically significant difference between treatment means. Survival rate was determined with a Kaplan-Meier survival curve, and the pairwise comparisons were made with log-rank (Mantel-Cox) and Gehan-Breslow-Wilcoxon tests. The survival analyses and graphs were plotted with GraphPad Prism v. 7 (GraphPad Software, La Jolla, CA, USA). LSD and one-way ANOVA were used to determine all variances. Heterogenous variances were analyzed with Welch (W), Brown-Forsythe (B), and Games-Howell tests. Rat body weights were repeated-measurement data and subjected to a correlated ANOVA.

Results

LXGYD improved short-term survival rate and general status of rats subjected to lethal dose of total body irradiation

LXGYD significantly prolonged short-term survival in irradiated rats (Figure 1A). Concentrated death occurred and only one rat each in the Radiation and Glu groups survived by the 10th day. Two and four rats in the M D and H D groups, respectively, survived after 2 weeks. The survival rates, median survival

times, and the numbers of deaths per group within 2 weeks after irradiation are shown in Figure 1A and Table S1.

LXGYD administration improved the general status of the irradiated rats except for their survival rates. At days 1–3 post-irradiation, the rats were relatively less active, and their fur became dry. Moreover, their food and water consumption sharply decreased. Pus and blood appeared in their feces and their eyelids bled in certain cases. The foregoing symptoms were severe for the Radiation group. The general status of the H D rats was slightly better than that of the other rats. In all groups, the average body weights significantly decreased after irradiation, reached their lowest levels by day 3 and began to rise thereafter but did not return to their initial levels. They continued to decline at ~9–10 d. The average body weights of the H D and M D rats were higher than that of the Radiation group on day 3 after irradiation ($P < 0.01$). By day 9 after irradiation, the average body weight of the H D rats was higher than that for the rats in the Radiation group ($P < 0.05$). (Figure 1B; Table S2). From D4 to D8, diarrhea ameliorated but the rats became inactive and bled from their eyelids or nasal cavities.

LXGYD promoted small intestinal tissue repair in rats subjected to a lethal dose of radiation

The rats were divided into groups and modeled, and the samples were collected at the corresponding time points (Figure 2A). Pathological analyses were performed at different time points to determine the extent of irradiation-induced intestinal injury and LXGYD-mediated repair (Figure 2B). HE staining on days 3, 5, and 10 post-irradiation showed that the epithelial cells of the intestinal villi of the rats in the Radiation group were swollen and had pale cytoplasm (Figure 2B; black arrow). Fibrous tissue proliferated in the submucosa and the gaps had widened (Figure 2B; purple arrow). There was extensive necrosis in the intestinal mucosa and diffuse inflammatory cell infiltration (Figure 2B; red arrow). The number of intestinal glands in the mucosal layer was significantly reduced and fibrous tissue proliferated in the glandular interstitium (Figure 2B; blue arrow).

For the Glu group, the epithelial cells of the intestinal villi were edematous and had light cytoplasms (black arrow). The crypt and intestinal gland structures were clear. Goblet cells were observed in the epithelial layer of the intestinal villi. Fibrous tissue proliferated in the submucosa and the gaps widened (purple arrow).

For the M D group, the epithelial cells of the intestinal villi were edematous and had light cytoplasms (black arrow). Inflammatory cell infiltration was observed in certain areas (red arrow). Some intestinal villi presented with microvascular hyperplasia and dilatation of the lamina propria (yellow arrow). The hierarchical structures of the intestinal mucosae, mucosal muscle layers, submucosae, and muscle layer of the rats in the H D group were clear. The epithelial cells of the intestinal villi in the mucosal layer were relatively intact and pathological changes in them were not obvious.

We also analyzed pathological changes at various time points after irradiation. Overall, the changes in the numbers of villi, crypt depth, and villus length were essentially the same after irradiation (Figure 2C, D, E). Compared with the Control, the number of villi, crypt depth, and villus length had significantly ($P <$

0.01) decreased on days 3, 5, and 10 after irradiation in the Radiation group. Pathological damage was the most severe on days 3 and 5 after irradiation in the Radiation group and the numbers of villi, crypt depth, and villus length were the lowest of all groups at this time. Damage to the intestinal mucosal was gradually restored in the Radiation group by day 10. Hence, the intestinal damage caused by irradiation at the experimental dose underwent a certain degree of self-repair, but the tissue was not restored to its normal mucosal structure.

HE staining showed that the intestinal structure of the Glu group was relatively healthy at 3–10 d after irradiation as a certain degree of intestinal wall thickening and epithelial cell edema had occurred. The effects of the irradiation on the numbers of villi, crypt depth, and villus length resembled those observed for M D ($P > 0.05$) but were more severe than those observed for H D ($P < 0.05$). The impact of irradiation was less severe in the Glu than the Radiation group and the former group gradually recovered.

Recovery was better for the medium-dose and high-dose groups than the Radiation group. In the former cases, cell morphology, numbers of villi, crypt depth, and villus length were relatively normal on the third day after irradiation. The pathological changes that occurred in the intestinal tract of the M D group gradually reversed over time. Nevertheless, some inflammatory cell infiltration and vascular dilation remained. By contrast, the H D group presented with relatively less inflammatory cell infiltration and no obvious tube wall thickening. Vascular dilatation and intestinal epithelial edema were observed in a few cases. Overall, treatment efficacy was highest for the Glu, M D, and H D groups in terms of the numbers of villi, crypt depth, and villus length ($P < 0.05$).

Active ingredients in LXGYD and network analysis of LXGYD

LC-MS was performed after drug decoction and concentration (Figure 3A). After network pharmacology analysis (Figure 3B), the top 100 compounds identified by semi-quantitation of positive and negative ions were selected for preliminary screening by setting the thresholds of the pharmacokinetic parameters in the TCMSP database as OB ≥ 30% and DL≥ 0.18. Thirteen active components in the compound were screened (Figure 4).

The overall pharmacological analysis of the network is shown in Figure 3B. We obtained 126 LXGYD targets from the TCMSP database. Correlations between these targets and the core molecules were demonstrated with Cytoscape (Figure 5A). The keywords “radiation induced intestinal injury” and “acute radiation syndrome” were used to query disease genes via the Genecard and OMIM databases. We obtained 478 targets after duplicates were removed and gene names were normalized. The targets were converted into common gene names through the UniProt database. Intersecting genes were identified with a Venn diagram (Figure 5B).

We analyzed the intersecting genes corresponding to the target of the active LXGYD component and the genes contributing to radiation-induced intestinal damage. Fifty-one common genes were potential LXGYD targets (Figure 5C). They were enriched by the String database and imported into Cytoscape for association analysis (Figure 5D). The target genes were enriched by the Metascape database for GO

analysis (Figure 5E). The GO BP showed that the 51 overlapping targets were associated with radiation-related biological processes such as cell apoptosis, cycle, differentiation, migration, and inflammatory response. The GO CC demonstrated that the foregoing targets focused on the cellular composition of enzymes regulating cyclin, cell membrane raft, transcription factors (TFs), nuclear envelope, basement membrane, spindle, and extracellular matrix. The GO MF revealed that the molecular functions of the intersecting targets focused on TF, phosphorylase, ubiquitin-specific protease, cytokine receptor, and NF-κB binding, and protein kinase and nuclear receptor activation. The KEGG enrichment analysis (Figure 5F) disclosed that ≥ 20 significant pathways were enriched including HSA04151PI3K, KO04064NF-κB, Wnt, and TJ. These were strongly correlated with acute intestinal radiation injury.

LXGYD may induce LGR5 $^{+}$ stem cell proliferation in the ileal crypts of rats by acting on the Wnt pathway

The network pharmacological analyses suggested the potential roles of the Wnt pathway in ileal crypt regeneration in irradiated rats. However, biological data are also required to validate these findings. CyclinD1 is implicated in intestinal repair under stress. Here, IHC staining of CyclinD1 (Figure 6A, B) showed that on day 3 after irradiation, CyclinD1 was significantly ($P < 0.01$) lower in the ileal crypts of the Radiation group than in those of the Control. CyclinD1 expression was higher in the H D group than the M D or Glu group ($P < 0.01$) and nearly 3× higher than that in the Radiation group ($P < 0.01$). CyclinD1 expression in the M D group was > 2× that of the Radiation group ($P < 0.01$). On day 5 after irradiation, there was no significant difference in CyclinD1 expression in the Radiation group compared with the Control. Nevertheless, the former presented with relatively shorter intestinal villi and disordered intestinal epithelial structure. Compared with the Control, CyclinD1 expression of was ≥2× higher in each of the treatment groups ($P < 0.01$). The order of CyclinD1 expression was M D > H D > Glu group. By day 10 after irradiation, CyclinD1 expression was significantly ($P < 0.01$) lower in the Radiation group than the Control but did not markedly differ from the Glu group. Relative CyclinD1 expression had significantly ($P < 0.01$) increased in the M D and H D groups. However, CyclinD1 expression was significantly ($P < 0.01$) higher in the H D than the M D group.

Lgr5 belongs in the Wnt pathway and is a pivotal intestinal stem cell marker. IHC (Figure 6C, D) showed that on the day 3 after irradiation, the number of Lgr5-positive cells in the ileal crypts of the Radiation group were significantly lower than those of the Radiation group. By contrast, Lgr5 was significantly ($P < 0.01$) upregulated in the ileal crypts of M D and H D groups. Lgr5-positive cells appeared mainly at the crypt bottom. Cell numbers were similar for both the M D and Control groups. Nevertheless, the cell number of the H D group was ≤ 1.5× that of the Control. On day 5 after irradiation, the Radiation group had ~1/2 as many Lgr5-positive cells as the Control ($P < 0.05$). Lgr5 expression in the H D group was > 3× that of the Radiation group. On day 10 after irradiation, the number of Lgr5-positive cells was significantly ($P < 0.01$) lower in the Radiation group than the Control. Compared with the Radiation group, there were significantly ($P < 0.01$) more Lgr5-positive cells in the M D and H D groups. The number of Lgr5-positive cells in the H D group was about the same as that for the Control ($P > 0.05$).

To confirm the involvement of the Wnt pathway in intestinal repair, we used western blotting to measure the expression levels of WNT3A, β-catenin, and C-MYC in irradiated rat intestine. These molecules are core factors in the Wnt classical pathway. Figure 7A, B shows that at every time point after irradiation, WNT3A, C-MYC and β-catenin were upregulated in the irradiated rats compared with the Control ($P < 0.01$).

Relative to the model control, glutamine had weaker therapeutic efficacy on day 3 after irradiation but stronger efficacy on days 5 and 10 after irradiation. The stimulatory effects of the M D and H D LXGYD treatments on the WNT pathway were stronger than that of glutamine immediately after radiation. The stimulatory effect of H D LXGYD was most evident at days 5 and 10 after irradiation ($P < 0.01$). On day 5 after irradiation, the stimulatory effect of the H D LXGYD treatment on the WNT pathway in irradiated GI-RS rats was ~5× stronger that of the Radiation group ($P < 0.01$). This stimulatory effect lasted ≤10 d after irradiation. The H D LXGYD treatment promoted the WNT pathway more strongly than the M D LXGYD treatment especially at days 5 and 10 after irradiation ($P < 0.01$).

We also detected the mRNA expression levels of Wnt-3A, C-MYC, and β-catenin (Figure 7C). The qRT-PCR results were essentially consistent with those of the WB. On the third day after irradiation, the Wnt-3A, C-MYC, and β-catenin transcription levels were significantly ($P < 0.05$) higher in the model group than the Control. Compared with the Radiation group, the glutamine treatment did not significantly promote Wnt-3A, C-MYC, or β-catenin transcription. The M D and H D LXGYD treatments were significantly ($P < 0.05$) more effective than the Glu treatment. Hence, the H D LXGYD treatment was the most efficacious especially on days 5 and 10 after irradiation ($P < 0.01$). However, the WNT-3A and β-catenin transcription levels were higher for the M D LXGYD treatment than the H D LXGYD treatment on day 3 after irradiation ($P < 0.01$).

LXGYD promoted TJ protein expression in intestinal epithelial cells via MEK/ERK pathway activation

On days 3, 5, and 10 after irradiation, we measured the *D*-lactic acid concentrations in the peripheral blood of all rats. *D*-lactic acid levels in the peripheral blood of the rats in the Radiation group, Glu, M D LXGYD and H D LXGYD groups were significantly ($P < 0.01$) higher than that of the control (Figure 8A). Compared with the Radiation group, the plasma *D*-lactic acid concentrations in the Glu group, M D LXGYD and H D LXGYD groups were significantly ($P < 0.01$) lower. The plasma *D*-lactic acid concentration was lowest for the H D LXGYD group. The *D*-lactic acid content in the peripheral blood gradually decreased with increasing time after irradiation ($P < 0.05$). Compared with day 3 after irradiation, the serum *D*-lactic acid content in the H D LXGYD group had significantly ($P < 0.01$) declined by day 5. However, the serum *D*-lactic acid content did not significantly ($P > 0.05$) differ between day 5 and day 10.

We performed semi-quantitative IHC staining to assess the effects of LXGYD on the intestinal epithelial cell TJ proteins, occludin and claudin-1 (Figure 8B–E). Compared with the control, the occludin content was significantly ($P < 0.01$) lower in each radiation treatment group. On day 3 after radiation, compared with the Radiation group, occludin was significantly ($P < 0.01$) upregulated in the LXGYD treatment group. Nevertheless, there were no significant ($P > 0.05$) differences in occludin content between the M D and H

D groups. On day 5 after irradiation, occludin was significantly upregulated in the M D, H D groups and Glu groups ($P < 0.01$ and $P < 0.05$, respectively). However, there was no significant difference ($P > 0.05$) in occludin expression between the Radiation and Glu groups. On day 10 after irradiation, compared with the Radiation group, occludin was significantly ($P < 0.05$) upregulated in the H D and M D groups. Nevertheless, there were no significant differences ($P > 0.05$) in occludin expression among the H D, M D, and Glu groups.

Claudin-1 was significantly ($P < 0.01$) downregulated in the Radiation group relative to that in the control. On day 3 after irradiation, claudin-1 was significantly ($P < 0.01$) upregulated in the MD group compared with the Radiation group and was significantly ($P < 0.01$) upregulated in the H D group compared with the Glu group. However, there was no significant ($P > 0.05$) difference in claudin-1 expression between the Glu and Radiation groups. On day 5 after irradiation, compared with the Radiation group, claudin-1 expression was higher for the H D group than the M D, Glu, and Radiation groups. Claudin-1 expression was highest for the H D groups and > 2× that of the Glu group. On day 10 after irradiation, claudin-1 was significantly ($P < 0.05$) upregulated in all treatment groups compared with the Radiation group. Claudin-1 expression in the H D group was ~4× higher than that of the Radiation group ($P < 0.01$).

Based on the previous reports and our network pharmacological analysis, we selected the MEK/ERK pathway as it expresses TJ proteins. We measured the expression levels of the key factors ERK, p-ERK, MEK, and p-MEK (Figure 9A, B). There were virtually no differences in ERK expression levels among groups on days 3, 5, and 10 after irradiation. On day 3 after irradiation, phosphorylated ERK expression level was significantly ($P < 0.01$) higher in the H D group than in the M D group and significantly ($P < 0.05$) higher than that in the other three groups. However, phosphorylated ERK expression did not significantly differ among the latter. MEK expression was significantly higher in the M D and H D groups than the other three. Nevertheless, there was no significant difference in MEK expression between the M D and H D groups. The p-MEK expression level was nearly zero in the control and very low in the Glu and H D groups. The latter two did not significantly differ in terms of p-MEK expression. However, p-MEK expression was significantly ($P < 0.01$) higher in the Radiation group and highest ($P < 0.05$) in the M D group ($P < 0.05$). At day 5 after irradiation, compared with the Control, the p-ERK expression level was lower in the Radiation group. However, p-ERK expression was relatively higher in the H D group followed by the Radiation, Glu, and M D groups. The p-ERK expression levels did not significantly differ between the Radiation and Glu groups but did significantly ($P < 0.01$) differ among the other groups. MEK expression was higher in the H D than the M D group. MEK expression was higher in the Glu than the Radiation and Control groups ($P < 0.01$). MEK expression did not significantly differ between the Glu and M D groups but did significantly differ among the other groups ($P < 0.01$). The p-MEK expression was highest in the H D group, followed by the M D, Glu, and Radiation groups. In the Control, there was virtually no p-MEK expression. Nevertheless, there were significant differences in p-MEK expression between these any 2 of the 4 groups ($P < 0.01$). p-ERK expression was significantly ($P < 0.01$) higher in the H D group than in the Glu, Radiation, and control groups. Nevertheless, there were no significant differences in p-ERK expression among the latter three groups or between the M D and H D groups. The MEK expression level was lowest for the Control and highest for the M D group followed by the H D, Glu,

and Radiation groups. There was no significant difference in MEK expression between the H D and Glu groups, but there were significant differences in MEK expression among the other groups ($P < 0.05$). The p-MEK expression level was highest for the H D group followed by the M D, Glu, Radiation, and Control group. In the latter case, p-MEK expression was nearly zero. there were significant differences in p-MEK expression between these any 2 of the 4 groups ($P < 0.01$).

Discussion

We empirically demonstrated that LXGYD promoted the repair of radiation-induced intestinal damage and improved survival in GI-ARS rats. LXGYD stimulated stem cell proliferation in the small intestine, upregulated TJ proteins, and reconstituted the ileal structure. Moreover, it may have activated the WNT and MEK/ERK pathways.

Radiation induces severe ISC injury during pathological GI-ARS progression[12]. Restoring ISC function after irradiation may help re-establish intestinal homeostasis, alleviate acute GI-ARS symptoms, and improve short-term survival[13]. However, the mechanisms underlying the protective effects of anti-radiation drugs such as LXGYD are unknown.

Wang et al.[14] reported that leukemia inhibitory factor (LIF) significantly affected the intestinal epithelia of both irradiated LIF-KO and WT mice. However, the damage was far more severe in the former. Post-irradiation LIF administration activated the AKT/GSK3β pathway and promoted ISC proliferation and intestinal epithelial regeneration. Chen et al.[15] established a GI-ARS animal model using 15 Gy local irradiation. TIGAR upregulation accelerated ISC division at the crypt bottom, thereby, promoting intestinal reconstruction after lethal-dose irradiation. Kalita Bhargab et al.[16] confirmed that the combined use of podophyllotoxin and rutin improved radiation-induced ISC damage possibly by upregulating the Wnt/β-catenin signaling pathway. Bhanja Payel et al.[17] found that in KO mice and organoid cultures, the antitumor drug BCN057 spared the ISC after lethal-dose irradiation, promoted intestinal epithelium regeneration, alleviated acute symptoms, and improved short-term survival. Wang Sihan et al.[18] demonstrated that subcutaneous Me6 injection in mice subjected to lethal-dose irradiation significantly increased intestinal crypt and villus length by promoting intestinal epithelial cell proliferation. The organoid culture showed that Me6 significantly increased budding. The study indicated that β-catenin is an important downstream target of Me6 and promotes post-irradiation ISC proliferation.

The present study demonstrated the protective efficacy of LXGYD against radiation-induced intestinal damage. LXGYD increased intestinal crypt number and depth and villus length and ameliorated pathological damage. The high LXGYD dose more effectively repaired post-irradiation ileal injury and improved survival than the medium LXGYD dose. Hence, the HD LXGYD may be a more suitable therapy for post-irradiation intestinal damage. The therapeutic efficacy of the new formula on animal survival and intestinal injury after radiation was similar to or even better than that of the original formula. Thus, the next steps were to identify the active principles in the prescription and elucidate their pharmacological modes of action.

The LXGYD was boiled and concentrated to produce two different dosages. The drug liquids were then analyzed by LC-MS. The output was filtered and 13 different active ingredients were screened. Fifty-one putative target genes were identified by finding the intersection between the targets of the foregoing active constituents and those in the GI-ARS database. KEGG and GO enrichment analyses were performed on these genes and the mechanism of pathological damage in GI-ARS was evaluated to rule out those reported in previous studies. We verified that the therapeutic mechanism of LXGYD involved the WNT pathway which affects intestinal repair by ISC. The KEGG enrichment analysis showed that LXGYD may regulate TJ protein expression. The KEGG enrichment and GO MF analyses suggested that phosphorylase binding may be associated with the LXGYD mode of action. We selected the phosphorylation pathway as it may affect TJ protein expression and is closely related to the PI3K/AKT and MEK/ERK pathways. The literature indicated that there is a cross-linking mechanism between WNT and MEK/ERK in ISC[19].

Our research team conducted preliminary clinical and experimental trials on the original prescription for the prevention and treatment of radiation-induced lung injury and enteritis[20]. The prescription was amended based on a Chinese herbal medicine formulated to treat radiation injury and the relevant therapeutic principles of TCM. A novel prescription was formulated with the intention to test its efficacy and elucidate its mechanisms in GI-ARS therapy.

In recent years, TCM has been widely applied in modern pharmacological research as it is cost-effective, has multiple targets, and involves numerous pathways. Based on the basic “JunChen ZuoShi” theory (The principle of combination of Chinese herbs) of TCM, different traditional Chinese medicines are often combined, and various preparation methods are used in clinical practice to achieve comprehensive therapeutic efficacy, improve the curative effect, and reduce toxicity. Nevertheless, the active components in TCM formulations are complex. For this reason, we implemented network pharmacology and omics techniques to explain the molecular-level mechanisms of TCM formulations based on the complex interactions among targets, biological functions, and bioactive compounds. This methodology transforms the study of TCM compounds from empiricism to objective data analysis. The latter approach generates relatively more evidence and supports a higher degree of consensus. The comprehensiveness, systematization, and integrity of network pharmacology conforms to the multi-drug and multi-target characteristics of TCM prescriptions.

This study clarified the potential impact of LXGYD on pathways that protect against radiation injury. We selected both the classical WNT stem cell proliferation and the MEK/ERK pathways. We chose the latter as it is closely related to TJ protein expression. Network pharmacology also revealed that the PI3K/AKT pathway was strongly correlated with the LXGYD mechanism. We detected a cross-linking effect between the PI3K and MEK/ERK pathways and mutual MEK/ERK and WNT pathway activation. Hence, the MEK/ERK pathway was selected for our investigations.

There were certain limitations to the current study. Significant progress has been made in the development of drugs such as small molecule compounds and free radical scavengers to treat radiation

injury. However, the US FDA has approved no drug for GI-ARS therapy. Glutamine is the most abundant amino acid in the serum. It is absorbed by the jejunum in response to intestinal injury and promotes intestinal epithelial cell proliferation[21]. However, it has not yet been evaluated as an independent clinical drug therapy strategy for GI-ARS. Hence, the selection of glutamine as a positive drug has certain limitations. Several studies showed that it promotes Lgr5+ ISC[22]. In a Glutamine-deficient environment, Lgr5+ISCs remain static while reactivated when the medium is replenished with Glutamine. As glutamine promotes ISC proliferation, increases crypt formation, and maintains intestinal homeostasis[23], we selected it as a positive drug in this study.

The present work disclosed inconsistent differences between the medium and high LXGYD doses. Overall, pathway activation, ISC proliferation, intestinal injury recovery, and TJ protein expression were higher for the H D than the M D group. In terms of other metrics, though, the M D treatment performed at least as well as the H D treatment. These discrepancies might have been caused by differences among individual experimental animals. Moreover, the high-dose LXGYD was too concentrated to be administered in a single gavage dose. When the rats coughed, gavage had to be interrupted and was resumed only after the coughing abated. Therefore, it is possible that the full drug dose was not effectively administered.

Despite its promise, network pharmacology has certain limitations. The existing database is incomplete. Furthermore, the application of network pharmacology in compound studies is mainly qualitative. As there are dosing effect relationships between drugs and diseases, currently available network pharmacology is not yet suitable for quantification.

Conclusions

We examined the active components of LXGYD and verified its possible action mechanism on intestinal stem cells and signal pathways of a GI-ARS rat model. LXGYD treatment improved the recovery of GI-ARS-induced rats. Moreover, LXGYD promoted ISC proliferation and tight junction protein expression through activation of the WNT and MEK/ERK pathways(Figure 10). Therefore, LXGYD has a positive therapeutic effect on GI-ARS and has the potential for further development and clinical application.

List Of Abbreviations

ELISA, enzyme-linked immunosorbent assay

GI-ARS, gastrointestinal acute radiation injury syndrome

IHC, immunohistochemistry

ISC, intestinal stem cell

LC-MS, liquid chromatography-mass spectrometry

LXGYD, Liangxue-Guyuan-Yishen decoction

RT-qPCR, real-time quantitative polymerase chain reaction

TJ, tight junction

WB, western blotting

TCM, traditional Chinese medicine

Declarations

Ethics approval

Animals were purchased from SPF (Beijing) Biotechnology Co. Ltd., Beijing, China. All animal experiments complied with relevant experimental animal welfare principles, which were approved by the Ethics Committee of the Academy of Military Medical Science, Beijing, China (No. IACUC-DWZX-2020-783).

Consent for publication

Not applicable.

Availability of data and materials

The datasets used and/or analyzed during the current study are available from the corresponding author on reasonable request.

Competing interests

The authors declare no competing financial interests.

Funding

The authors declare that they have received no funding for this study.

Authors' contributions

ZQY and BFY contributed equally to this work by conceiving the study, performing the experiments, and writing the manuscript supervised by YQD and HZ who revised the manuscript. YGW, JF, QYY and XL participated in the data acquisition and interpretation. All authors read and approved the final manuscript.

Acknowledgements

Not applicable

References

1. Chapel A, Francois S, Benderitter M , et al. New insights for pelvic radiation disease treatment:Multipotent stromal cell is a promise mainstay treatment for the restoration of abdominopelvic severe chronic damages induced by radiotherapy[J]. World J Stem Cells, 2013(4):106-106.
2. Qiu W, Leibowitz B, Zhang L, et al. Growth factors protect intestinal stem cells from radiation-induced apoptosis by suppressing PUMA through the PI3K/AKT/p53 axis[J]. Oncogene, 2010.
3. Liang W, Leibowitz B J, Xinwei W, et al. Inhibition of CDK4/6 protects against radiation-induced intestinal injury in mice[J]. Journal of Clinical Investigation, 2016, 126(11):4076-4087.
4. Bhanja P , Norris A, Gupta-Saraf P, et al. BCN057 induces intestinal stem cell repair and mitigates radiation-induced intestinal injury[J]. Stem Cell Research & Therapy, 2018, 9(1):26.
5. MAISIN, J. R . Bacq and Alexander Award lecture–chemical radioprotection: past, present, and future prospects.[J]. International Journal of Radiation Biology & Related Studies in Physics Chemistry & Medicine, 1998, 73(4):443-450.
6. Wang An,Wang Lei,Lu Xi et al. A Chinese herbal prescription Yiqi Jiedu decoction attenuates irradiation induced testis injury in mice.[J] .Biomed Pharmacother, 2020, 123: 109804.
7. Wang Ziwen,Chen Zelin,Jiang Zhongyong et al. Cordycepin prevents radiation ulcer by inhibiting cell senescence via NRF2 and AMPK in rodents.[J] .Nat Commun, 2019, 10: 2538.
8. Liang Jia-Wu,Li Pei-Lin,Wang Qian et al. Ferulic acid promotes bone defect repair after radiation by maintaining the stemness of skeletal stem cells.[J] .Stem Cells Transl Med, 2021, 10: 1217-1231.
9. Yin Peng,Zhang Zhicong,Li Jiandong et al. Ferulic acid inhibits bovine endometrial epithelial cells against LPS-induced inflammation via suppressing NK-κB and MAPK pathway.[J] .Res Vet Sci, 2019, 126: 164-169.
10. Das Ujjal,Manna Krishnendu,Adhikary Arghya et al. Ferulic acid enhances the radiation sensitivity of lung and liver carcinoma cells by collapsing redox homeostasis: mechanistic involvement of Akt/p38 MAPK signalling pathway.[J] .Free Radic Res, 2019, 53: 944-967.
11. Wang Yuguo,Dou Yongqi,Feng Jian et al. Efficacy of Liangxue Guyuan decoction on radiation-induced intestinal injury in rats via the toll-like receptor 4/myeloid differentiation primary response 88/ nuclear factor-kappa B pathway.[J] .J Tradit Chin Med, 2021, 41: 254-261.
12. Withers HR. Regeneration of intestinal mucosa after irradiation. Cancer 1971; 28:75–81.
13. Hauer-Jensen M, Wang J, Boerma M, Fu Q, Denham JW. Radiation damage to the gastrointestinal tract: mechanisms, diagnosis, and management. Curr Opin Support Palliat Care 2007; 1: 23-29
14. Wang Huaying,Wang Jianming,Zhao Yuhan et al. LIF is essential for ISC function and protects against radiation-induced gastrointestinal syndrome.[J] .Cell Death Dis, 2020, 11: 588.
15. Chen Fei,Zhang Yushuo,Hu Songling et al. TIGAR/AP-1 axis accelerates the division of Lgr5 reserve intestinal stem cells to reestablish intestinal architecture after lethal radiation.[J] .Cell Death Dis, 2020, 11: 501.

16. Kalita Bhargab,Ranjan Rajiv,Gupta Manju Lata,Combination treatment of podophyllotoxin and rutin promotes mouse Lgr5 intestinal stem cells survival against lethal radiation injury through Wnt signaling.[J] .Apoptosis, 2019, 24: 326-340.
17. Bhanja Payel,Norris Andrew,Gupta-Saraf Pooja et al. BCN057 induces intestinal stem cell repair and mitigates radiation-induced intestinal injury.[J] .Stem Cell Res Ther, 2018, 9: 26.
18. Wang Sihan,Han Yi,Zhang Jing et al. Me6TREN targets β-catenin signaling to stimulate intestinal stem cell regeneration after radiation.[J] .Theranostics, 2020, 10: 10171-10185.
19. Wei G, Gao N, Chen J , et al. ERK/MAPK signaling is essential for intestinal development through Wnt pathway modulation[J]. Development, 2020, 147(17):dev.185678.
20. Dou Y Q, Yang M H, Wei Z M , et al. The Study of Early Application with Dixiong Decoction (□□□)for Non-small Cell Lung Cancer to Decrease the Incidence and Severity of Radiation Pneumonitis: A Prospective,Randomized Clinical Trial[J]. Chinese Journal of Integrative Medicine, 2010, 016(005):411-416.
21. Beaufrere, A.M.; Neveux, N.; Patureau Mirand, P .; Buffiere, C.; Marceau, G.; Sapin, V .; Cynober, L.;Meydinal-Denis, D. Long-term intermittent glutamine supplementation repairs intestinal damage (structureand functional mass) with advanced age: Assessment with plasma citrulline in a rodent model. J. Nutr.Health Aging 2014, 18, 814–819.
22. Moore, S.R.; Guedes, M.M.; Costa, T.B.; Vallance, J.; Maier, E.A.; Betz, K.J.; Aihara, E.; Mahe, M.M.; Lima, A.A.;Oria, R.B.; et al. Glutamine and alanyl-glutamine promote crypt expansion and mTOR signaling in murine enteroids. Am. J. Physiol. Gastrointest. Liver Physiol. 2015, 308, 831–839.
23. Chen Yun,Tsai Ya-Hui,Tseng Bor-Jiun et al. Influence of Growth Hormone and Glutamine on Intestinal Stem Cells: A Narrative Review.[J] .Nutrients, 2019, 11: undefined.

Figures

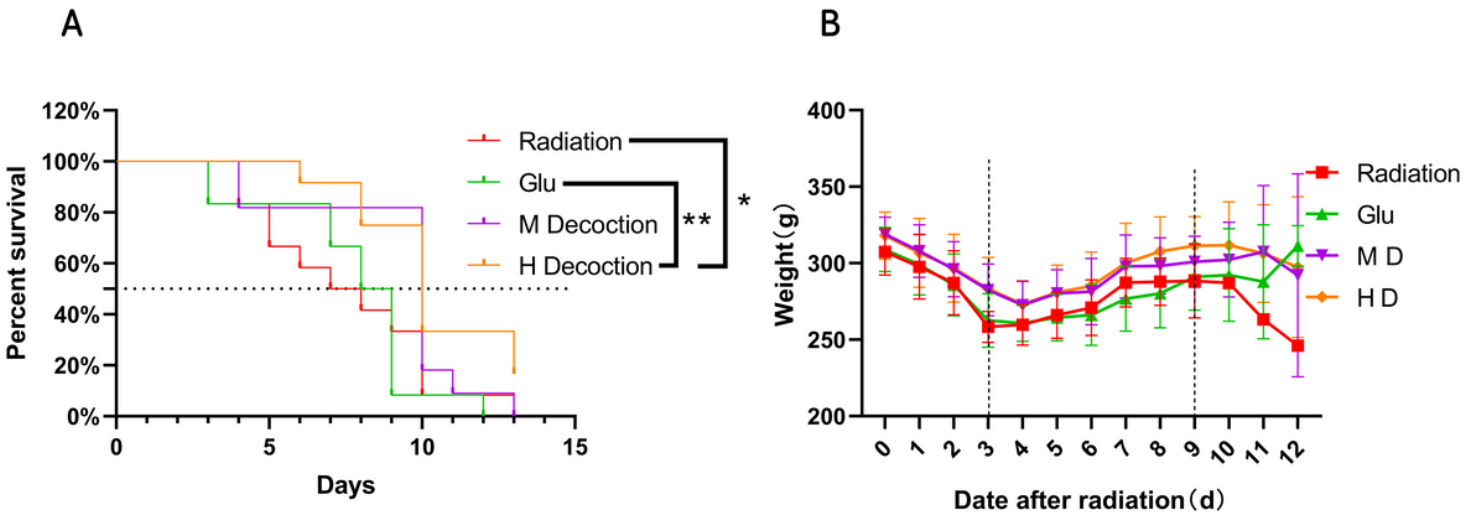

Figure 1

LXGYD can improve the short-term survival rate and survival status of rats after total body irradiation with lethal dose (A) Survival curves of rats in different treatment groups after 10 Gy total body irradiation from CO60-γ radiation source (n=12). (B) Weight change curve of rats in different treatment groups after 10 Gy total body irradiation from CO60-γ radiation source.

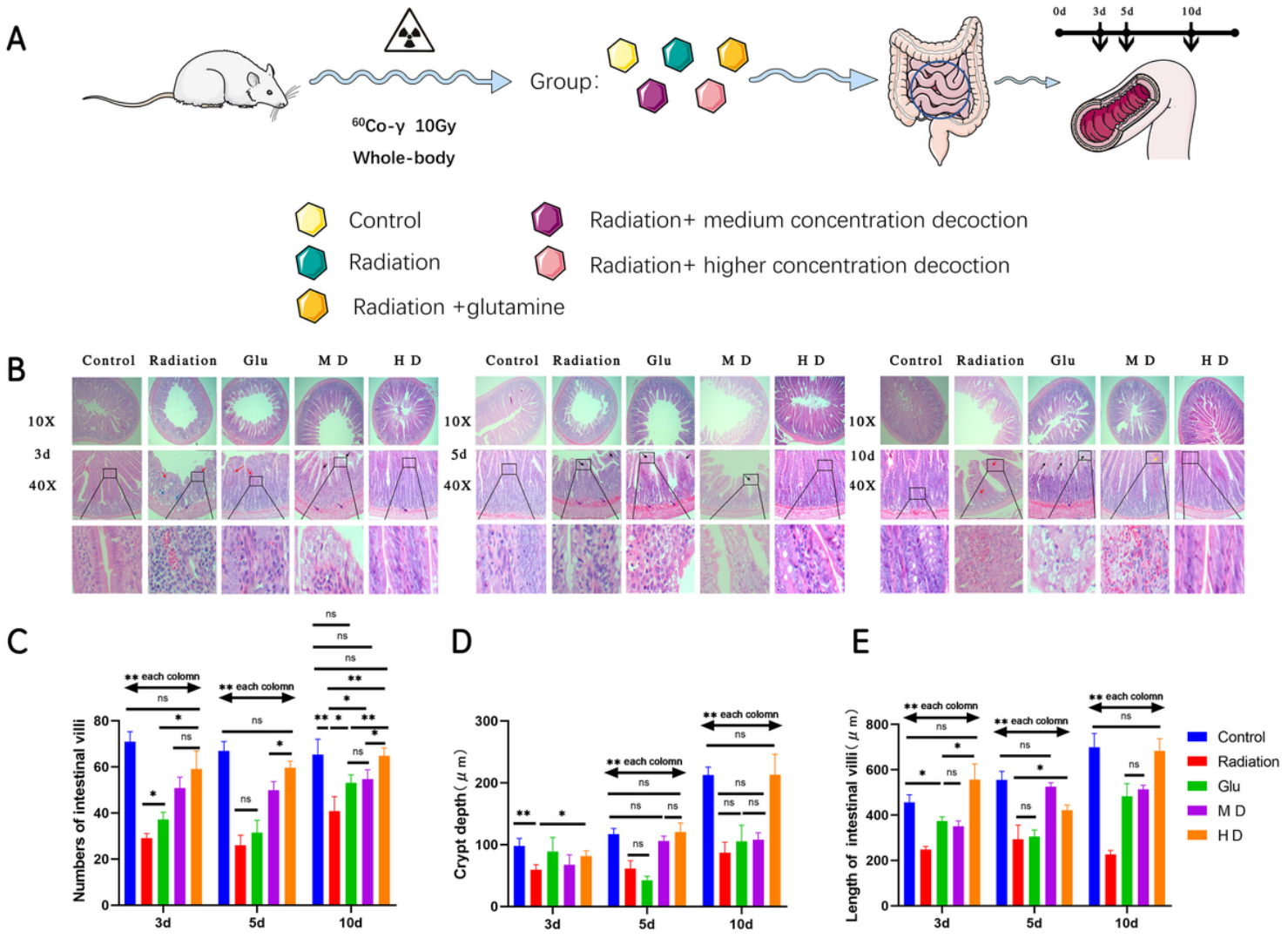

Figure 2

Experimental model, Hematoxylin-eosin staining and quantification of villus number, length, and crypt depth (A) Male SD rats (n=85; 280−-300 g) were randomly divided into control, radiation, radiation + glutamine (Glu), radiation + medium concentration decoction (M D), and radiation + higher concentration decoction (H D) groups. After adaptive feeding for 3 d, rats were fasted for 8 h before irradiation. Excluding the control, all groups were subjected to single whole-body irradiation with 10-Gy of 60Co γ-rays (source to dermal distance = 3 m). From day 1 post-irradiation, the control and radiation groups were given normal saline (10 ml/kg), and the Glu group was given glutamine suspension (10 ml/kg, 0.3 g/mL). Five rats were randomly selected at the 3rd, 5th and 10th day post-irradiation (2.73 g/mL and 5.46 g/mL in the M D and H D groups, respectively). After abdominal aorta blood collection, the rats were anesthetized and sacrificed and 5 cm of jejunum and bilateral femur were dissected and interpreted. (B)

Representative Hematoxylin-eosin staining sections of jejunum 3, 5 and 10 days after 10-Gy total body irradiation in different treatment groups. Quantification of villus number (C), length (D) and crypt depth (E). Bars in A represent 500 and 200 μm, respectively, *P < 0.05, **P < .01

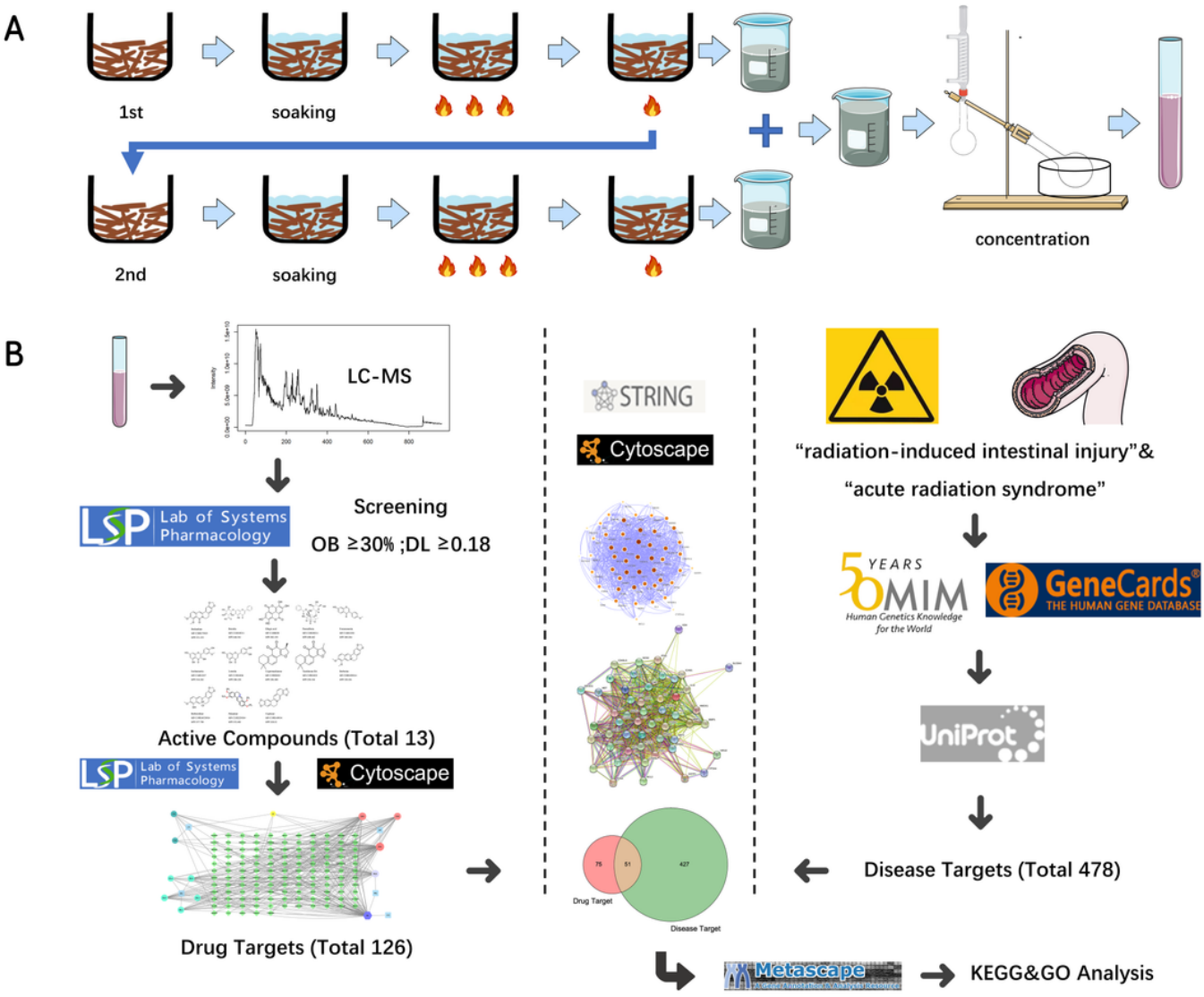

Figure 3

Drug preparation and network pharmacological study (A) The drug was prepared, adjusted to the appropriate concentration, and stored at 4 °C. (B) The network pharmacological study procedure.

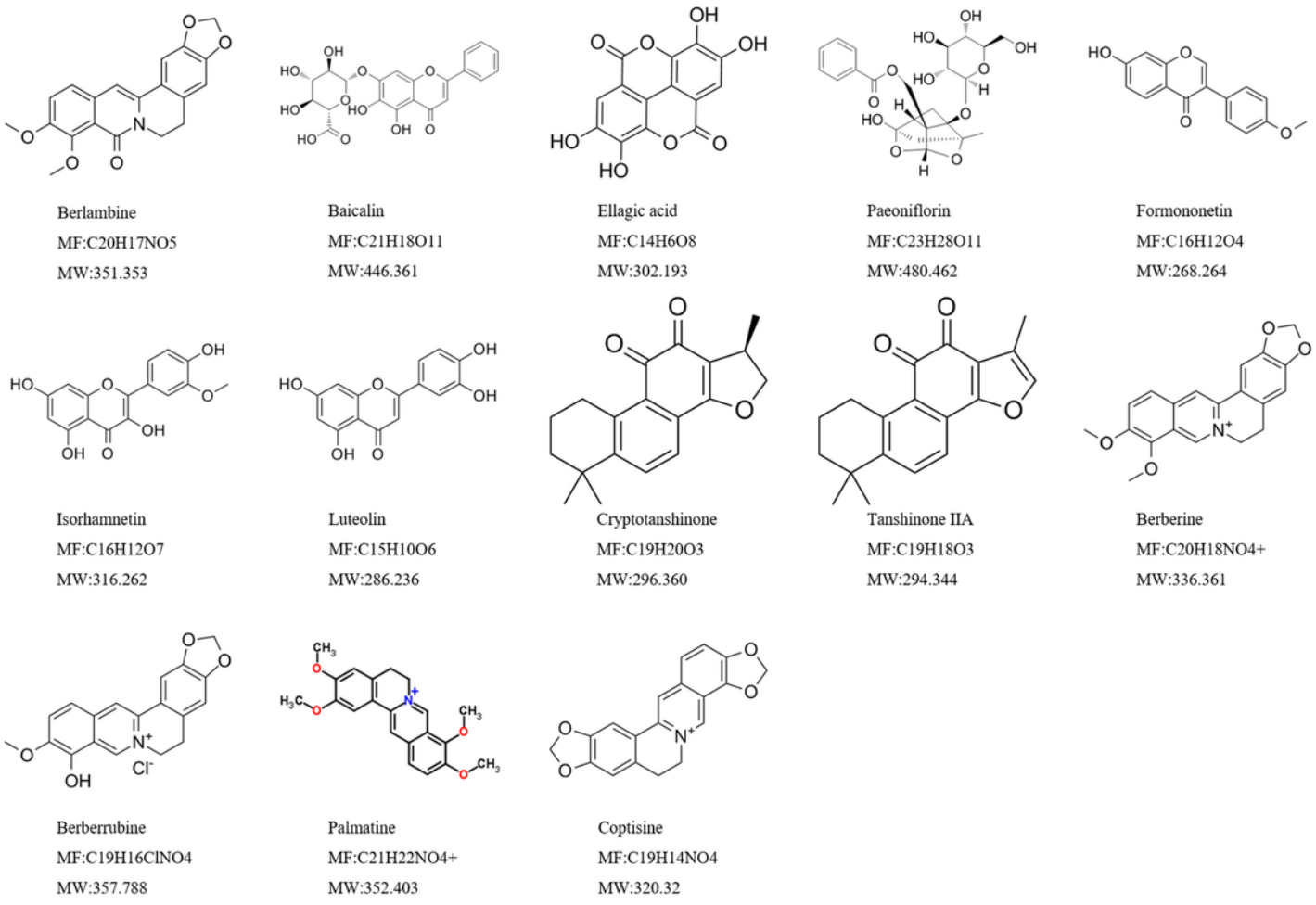

Figure 4

Active components within Liangxue-Guyuan-Yishen decoction (LXGYD) According to an oral bioavailability ≥ 30% and drug-likeness ≥ 0.18, 13 active components in LXGYD were screened.

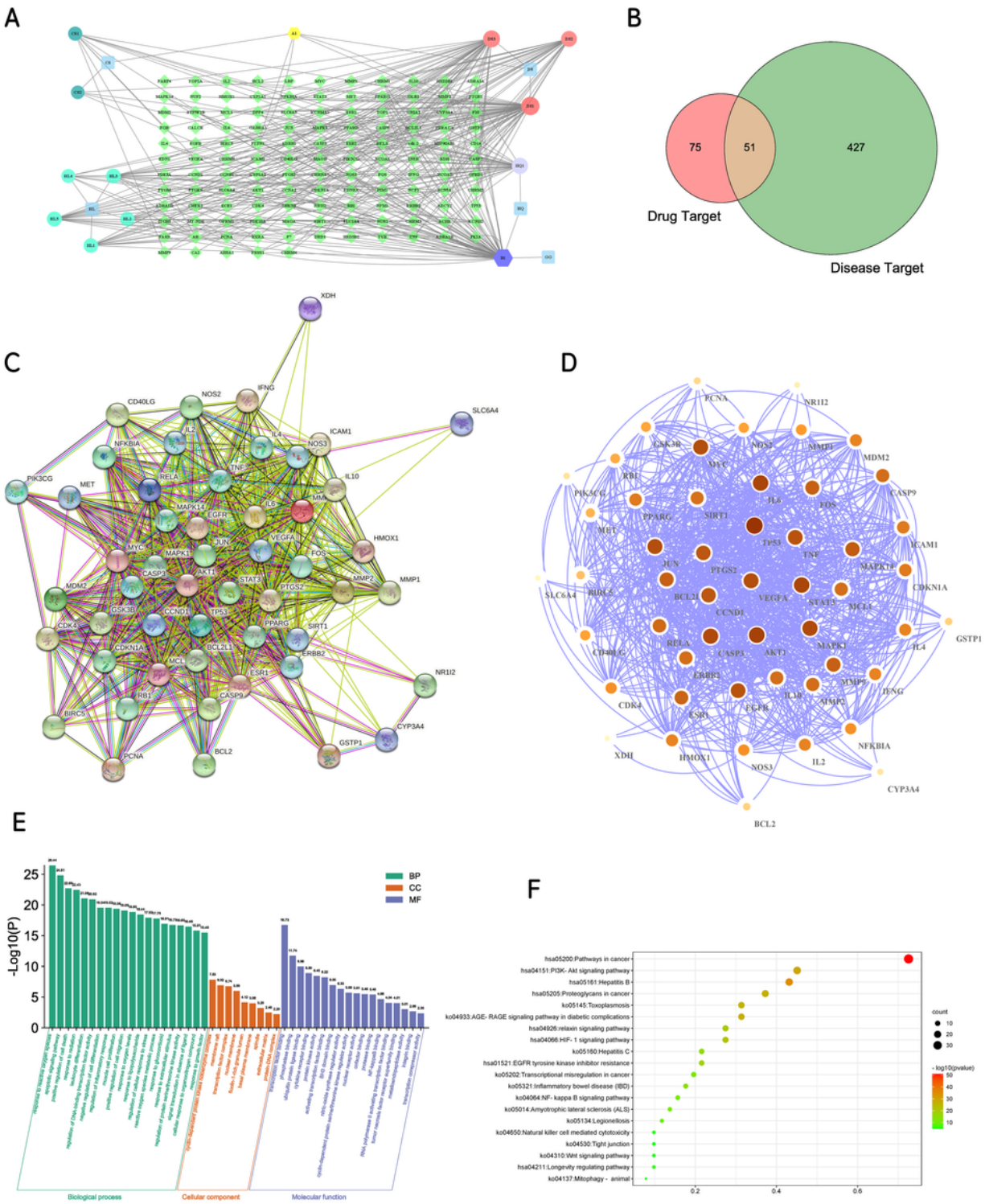

Figure 5

Correlation analysis, Venn diagram, interaction network, cytoscape map, GO and KEGG enrichment analyses of intersecting genes. (A) Target interaction relationship of core active components Among them, light blue is the main drug (CS: red peony root, HL: coptis, DS: salvia miltiorrhiza, GG: pueraria root, HQ:Astragalus membranaceus), dark green is the active ingredient of CS (CS1: Ellagic acid, CS2: Paeoniflorin), lighter blue for the effective ingredient of HL (HL1: Berberine, HL2: Berberrubine, HL3,

Palmatine, HL4, Coptisine, HL5: Berlambine,), red for the DS effective components (DS1: Luteolin, DS2: Cryptotanshinone, DS3: Tanshinone IIA,), lilac is the active component of HQ (HQ1: Isorhamnetin), purple is the common component of HQ and GG (B1:Formononetin), and yellow is the common component of CS and DS (A1: Baicalin). (B) The intersecting gene disease target and core active component gene target. (C) The interaction network of the intersecting genes□Colored nodes: query proteins and first shell of interactors□white nodes: second shell of interactors; empty nodes: proteins of unknown 3D structure; filled nodes: some 3D structure is known or predicted; edges: known interactions (light blue: from curated databases; purple: experimentally determined), predicted interactions (green: gene neighborhood; red: gene fusions; blue: gene co-occurrence), others (yellow: textmining; black: co-expression; lavender: protein homology). (D) Cytoscape map of the intersecting genes; node color and size represent how close the connections are. GO enrichment analysis (E) and KEGG enrichment analysis (F) of the intersecting genes.

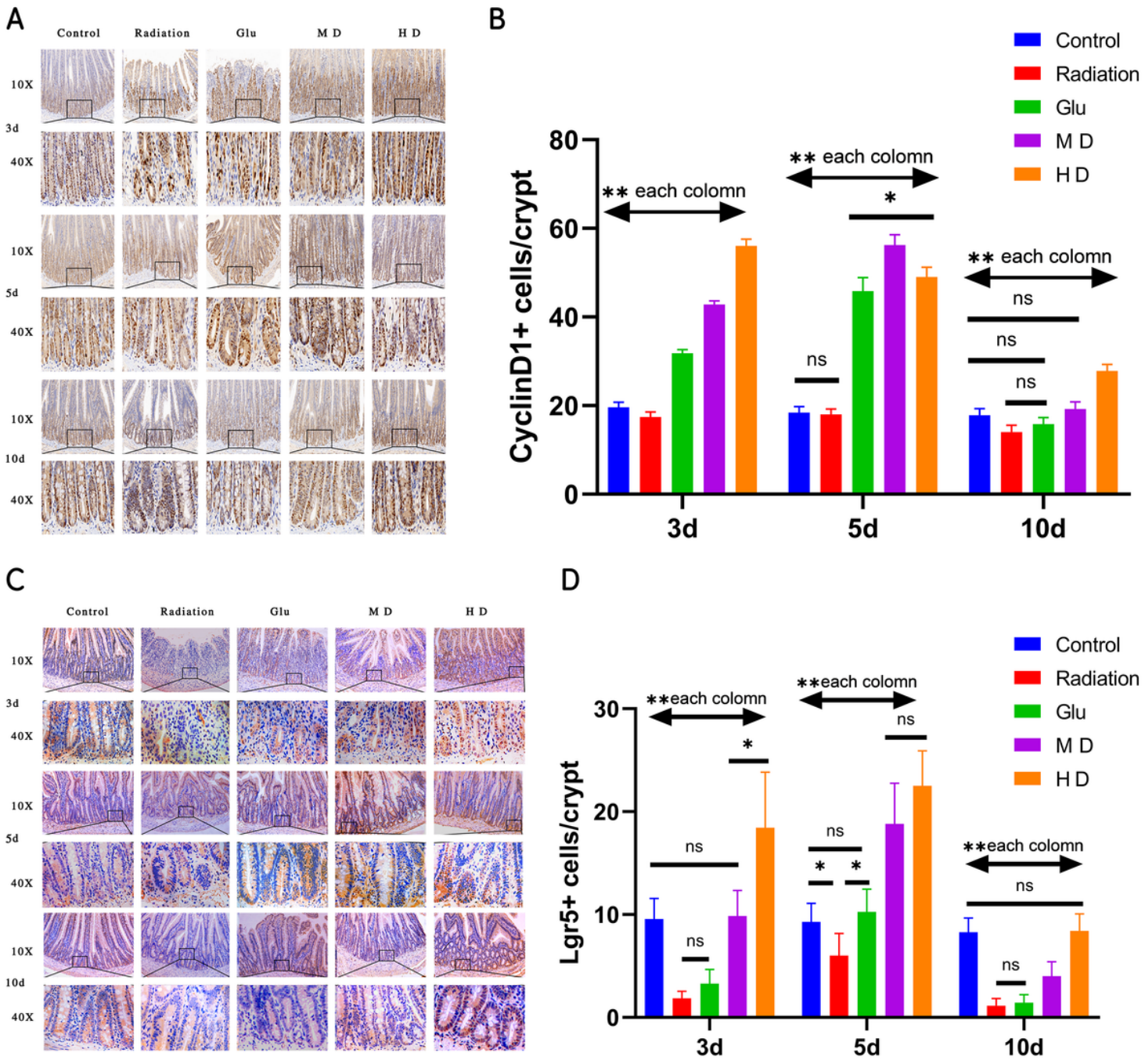

Figure 6

Immunohistochemical staining and a comparison between Lgr5+ cells/crypt and CyclinD1+ cells /crypt among the experimental groups (A,B) Immunohistochemical staining of CyclinD1 in cells at the bottom of the crypt showed that two concentration gradients of Liangxue-Guyuan-Yishen decoction (LXGYD) and glutamine could significantly increase CyclinD1 expression levels in crypt cells, especially on the day 3 and 5 post-radiation. LXGYD showed an improved treatment effect over that of glutamine. Bars in A represent 200 and 50 μm, respectively; *P<0.05, **P<.01. (C, D) Immunohistochemical staining of Lgr5+ cells in cells at the bottom of the crypt showed that two concentration gradients of LXGYD and glutamine can significantly improve Lgr5 expression levels in crypt cells, increase the quantity of Lgr5 + cells, and

maintain fossae status updates, especially on days 3 and 5 post-radiation. LXGYD showed an improved treatment effect over that of glutamine. Bars in C represent 200 and 50 μm, respectively; *P < .05,**P < .01

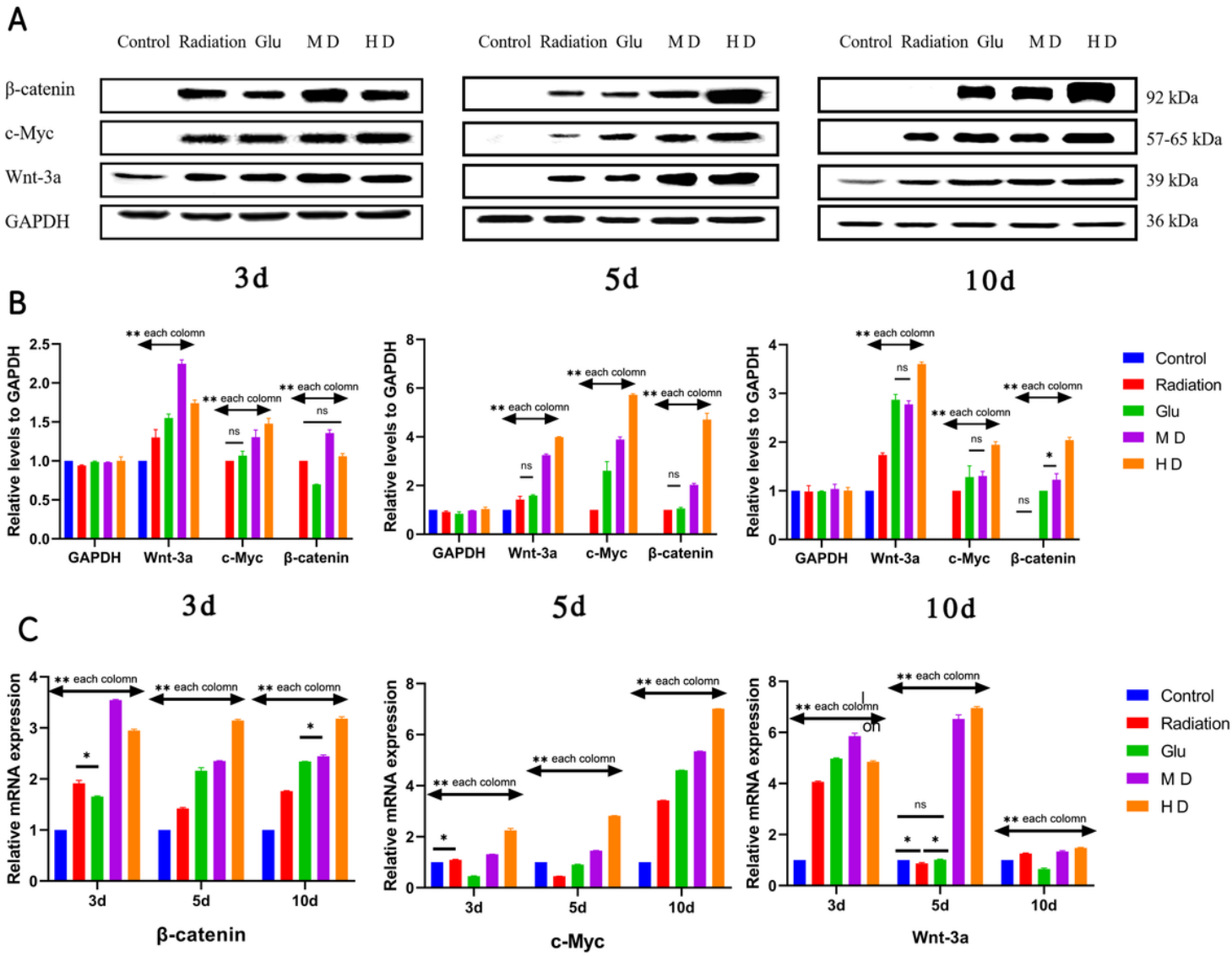

Figure 7

Western blot analysis and RT-PCR measuring relative mRNA expression levels of β-catenin, C-MYC, and Wnt-3A (A) Western blot results showed that irradiation could significantly activate the Wnt pathway in jejunal cells, and that irradiated small intestine tissue entered the repair state. (B) RT-PCR results showed that both Liangxue-Guyuan-Yishen decoction (LXGYD) and glutamine could up-regulate the Wnt pathway, but that LXGYD treatment increased the expression of β-catenin and C-Myc the most, compared to that of glutamine (*P < .05,**P < .01). C) RT-PCR results showed that Wnt-3a expression was significantly increased post-irradiation, and that LXGYD treatment up-regulated β-catenin and C-Myc*P < .05,**P < .01).

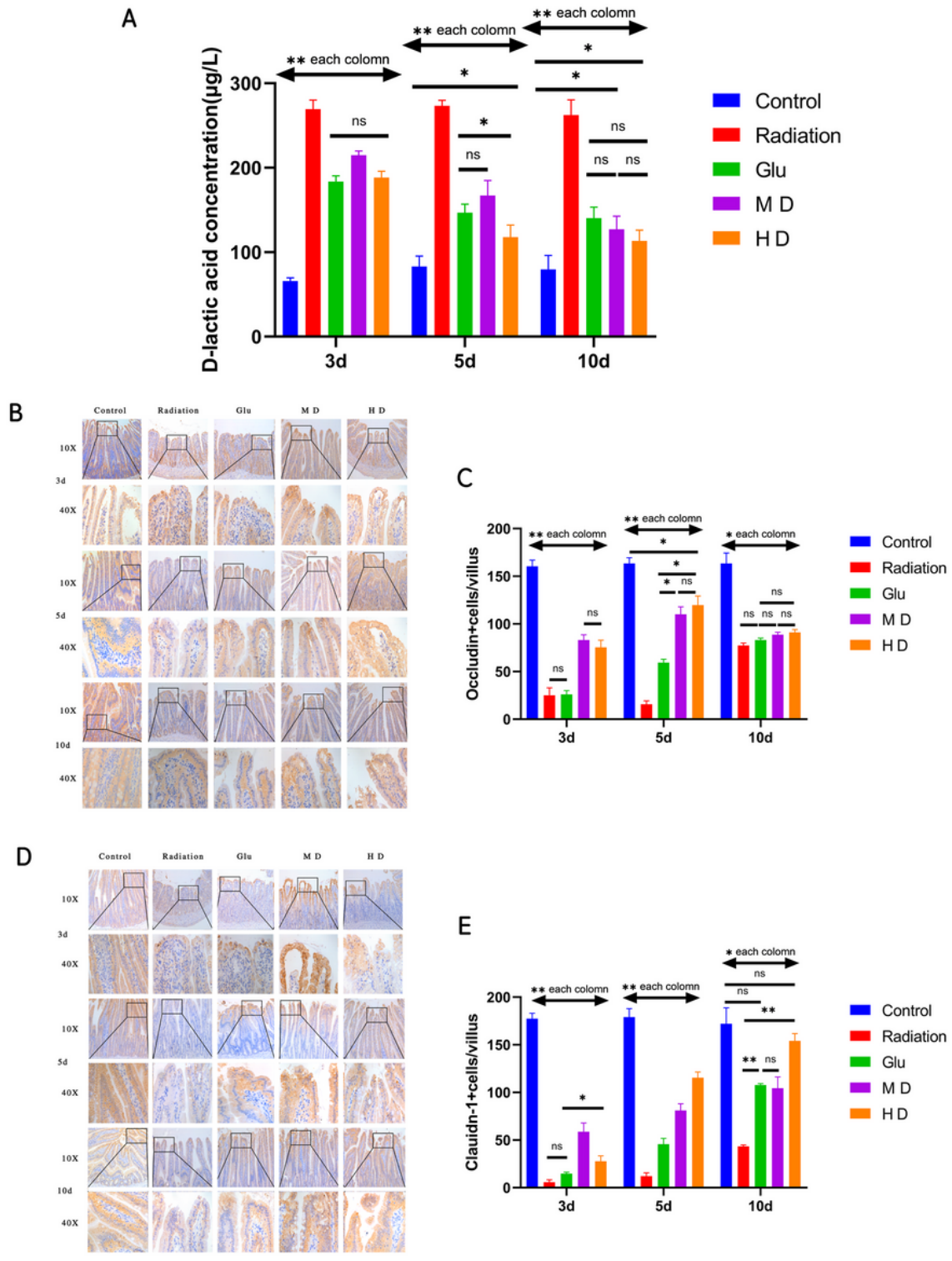

Figure 8

Enzyme-linked immunosorbent assay measuring D-lactic acid concentration and immunohistochemical staining of occludin and claudin-1 (A) Rat D lactic acid ELISA kit was used to detect the peripheral blood serum of rats (P < .05, **P < .01). (B, C) Immunohistochemical staining showed that the expression of tight junction proteins, occludin and claudin-1, in the jejunum epithelial cells was significantly reduced post-radiation. This could be party alleviated by Liangxue-Guyuan-Yishen decoction (LXGYD) and

glutamine, among which the effect of LXGYD was relatively better. Bars in A represent 200 and 50 μm, respectively, *P < 0.05, **P < 0.01.

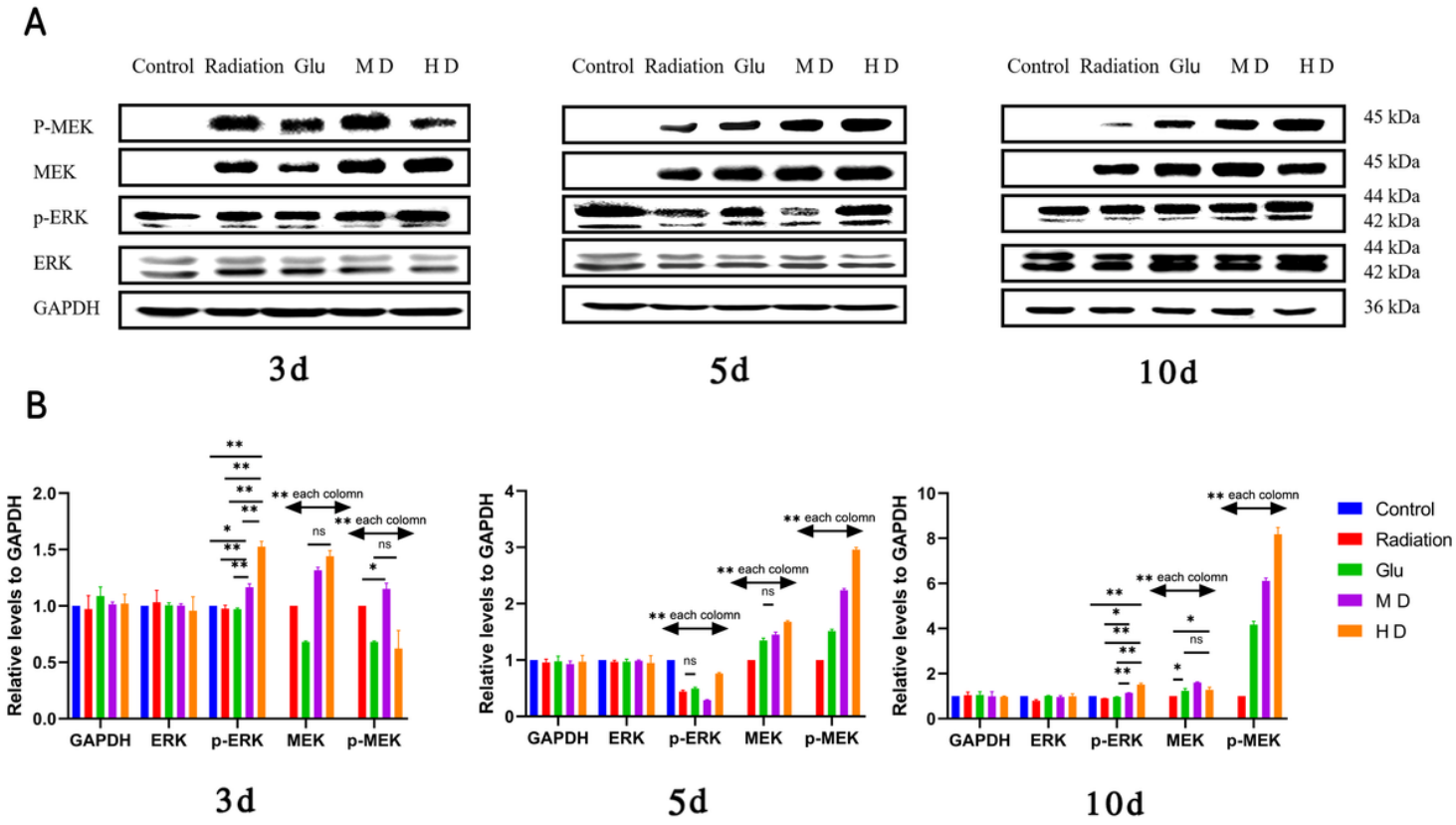

Figure 9

Western blot and semi-quantitative analyses of MEK/ERK pathway expression (A)The key factors in the MEK/ERK pathway, ERK, p-ERK, MEK and p-MEK, were detected by western blotting, and a semi-quantitative analysis was performed. (B) The MEK/ERK pathway could be activated and partially upregulated post-radiation, and Liangxue-Guyuan-Yishen decoction (LXGYD) treatment induces an increased upregulation of ERK, p-ERK, MEK, and p-MEK; especially on days 5 and 10 post-radiation (*P < 0.05, **P < 0.01).

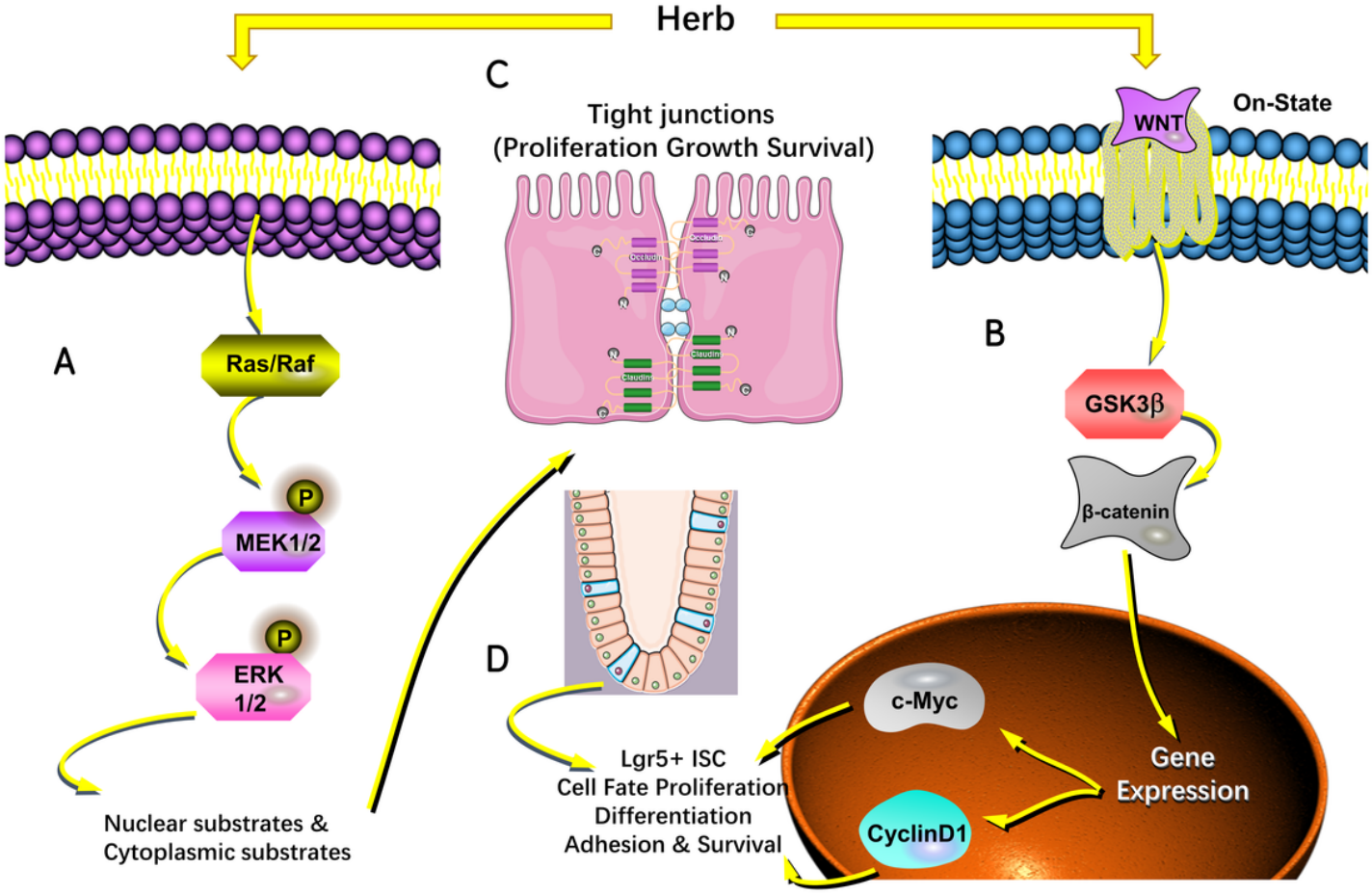

Figure 10

Suggested mechanism of action of Liangxue-Guyuan-Yishen decoction on the WNT and MEK/ERK pathways. The administration of Liangxue-Guyuan-Yishen decoction (LXGYD) had a good recovery effect on GI-ARS-induced rats. LXGYD treatment promoted intestinal stem cell (ISC) proliferation and tight junction protein expression through the activation of the WNT and MEK/ERK pathway.

Supplementary Files

This is a list of supplementary files associated with this preprint. Click to download.

- supplementaryfigures1.png
- supplementarytables.docx